

# Eutectic and peritectic equilibria in coherent binary alloys

Samiah Hassan<sup>a</sup>, Jiayang Wang<sup>a</sup>, Teddy Meissner<sup>b</sup>, Pierre A. Deymier<sup>a</sup>, Marat I. Latypov<sup>a,b,\*</sup>

<sup>a</sup>*Department of Materials Science and Engineering, University of Arizona, Tucson, AZ 85721, USA*

<sup>b</sup>*Graduate Interdisciplinary Program in Applied Mathematics, University of Arizona, Tucson, AZ 85721, USA*

---

## Abstract

This work extends the Cahn–Larché thermodynamic framework to binary alloys in which two coherent solid phases coexist with an incoherent liquid and investigates how coherency strain energy modifies classical eutectic and peritectic equilibria. We derive equilibrium conditions for three-phase coexistence that include an elastic energy term dependent on the molar fractions of the solid phases and apply them to model binary eutectic and peritectic systems. We find that coherency stress transforms the eutectic point into a finite three-phase equilibrium field spanning a continuous range of compositions and temperatures. In contrast, coherency stress in peritectic systems progressively destabilizes the two-solid equilibrium without generating a stable three-phase field and can suppress the peritectic reaction entirely. This asymmetry is governed by the geometric relationship between the stress-free compositions of the phases: when the liquid composition lies between those of the two solids (eutectic configuration), the liquid serves as a thermodynamic buffer against the coherency penalty on the solid–solid pair; when it lies outside (peritectic configuration), no such mechanism is available. These results demonstrate that coherency stress can fundamentally alter three-phase equilibria involving a liquid and suggest that such effects may be significant in systems with large coherent misfits.

*Keywords:* Thermodynamics of stressed solids, Coherency, Phase diagrams, Invariant points

---

## 1. Introduction

Coherency stress is a common feature of multi-phase crystalline solids in which phases share the same crystal structure across the interface but have different equilibrium lattice parameters [1]. Coherent interfaces are commonly found in technologically critical materials. Examples include Ni-base superalloys with the  $\gamma/\gamma'$  microstructure providing high-temperature strength [2]; age-hardened aluminum alloys and advanced steels strengthened with coherent precipitates [1]; and strain-engineered semiconductor heterostructures that exploit coherent epitaxy to tailor electronic band structure in devices based on Si–Ge, Ge–Sn, and III–V alloys [3, 4, 5]. Coherent microstructures are increasingly relevant with the rise of processing and

manufacturing methods that involve rapid solidification (e.g., metal 3D printing), which can preserve coherent interfaces between phases that would otherwise relax through misfit-dislocation formation under slower cooling [6].

The strain energy associated with an elastically accommodated lattice misfit between coherent phases contributes to the total free energy of the system and fundamentally alters the conditions for phase equilibria. The general framework for treating thermodynamics of stressed solids was established by Larché and Cahn in a series of foundational studies [7, 8, 9]. Applying this framework to a model binary system composed of two isotropic, elastically identical solid phases, Cahn and Larché [10] showed that coherency strains stabilize a single-phase solid solution relative to a two-phase mixture, that the classical common-tangent construction does not apply, and that the Gibbs phase rule no longer holds: the number of coexisting phases becomes independent of the classi-

---

\*corresponding author  
*Email address:* latmarat@arizona.edu (Marat I. Latypov)

cal thermodynamic degrees of freedom. Subsequent theoretical work by Johnson and Voorhees [11, 12] further elucidated the consequences of coherency stress, including the existence of multiple linearly stable equilibrium states under identical thermodynamic conditions. The predictions of the Larché–Cahn theory have received direct experimental confirmation by Shi et al. [13], who verified the open-system elastic parameters in nanoporous Pd–H using dynamic mechanical analysis and found excellent agreement with theory. More recent generalizations have extended the Cahn–Larché model to systems with free surfaces [14], large lattice mismatch [15], and elastic anisotropy [16].

Beyond phenomenological formulations based on the Cahn–Larché theory, coherent phase diagrams have been pursued with computational methods. Wood and Zunger [17, 18] introduced a first-principles approach using density functional theory and the cluster variation method to calculate coherent phase boundaries. More recently, Behara et al. [19] developed a statistical-mechanics framework coupling chemical ordering and mechanical strain from first principles to predict alloy phase stability under coherent conditions. Using the same approach, Jung et al. [5] examined how strain and composition affect the thermodynamic stability of Ge–Sn alloys and demonstrated new design spaces for strain-engineered semiconductor materials. Wang and Chen [20] developed a general thermodynamic theory for strain phase equilibria and diagrams applicable to diverse material systems including ferroelectrics and correlated oxides. Coherency stress effects have also been of continuing interest in the phase-field community, from the classical works of Khachaturyan with coworkers [21, 22, 23] to recent chemomechanical phase-field developments [24, 25].

Despite this extensive body of work, nearly all studies of coherency effects on phase equilibria have focused on fully solid-state systems. The implicit assumption has been that coherency stress is irrelevant to equilibria involving a liquid phase because liquids cannot sustain shear stress. However, this reasoning overlooks that the elastic strain energy penalty on the solid–solid pair coexisting with a liquid still contributes to the total system energy and can shift the conditions for phase equilibria.

Among the few studies to address this, Roytburd and Sung [26] showed that elastic interactions in a thin-film eutectic system grown epitaxially on a substrate alter the topology of the eutectic phase

diagram by splitting the eutectic point into two points or transforming it into a consolute point, depending on the sign of the elastic interaction energy between the phases. In all cases, three-phase coexistence in their model remains confined to isolated points in composition–temperature space. Our own prior work examined the effect of epitaxial strain on solid–liquid equilibria involving a chemical reaction [27] and on dissolution/crystallization of apatite under stress [28]. However, the effect of intrinsic coherency stress from lattice misfit between two solid phases on the classical invariant equilibria has not been investigated.

This gap is critical because eutectic and peritectic reactions govern solidification phenomena, including freezing ranges, solute partitioning between solid and liquid, as well as microstructural length scales. They also control the spatial extent of the mushy zone, which is the semi-solid region where liquid and solid coexist during casting, welding, and additive manufacturing [29, 30]. Classical models of eutectic and peritectic solidification rely on conventional stress-free phase diagrams [31, 32, 33] and thus overlook potential coherency effects.

To fill this gap, this study extends the Cahn–Larché framework to alloys in which two coherent solid phases coexist with an incoherent liquid. We derive equilibrium conditions for three-phase coexistence in the presence of coherency elastic strain energy (Section 2) and apply them to model eutectic and peritectic systems (Section 3). We show that coherency stress transforms classical eutectic points into finite three-phase equilibrium fields in composition–temperature space and, in contrast, destabilizes the two-solid equilibrium in peritectic systems. This asymmetry, which has not been previously reported, defines new thermodynamic bounds for solidification and offers a mechanistic basis for interpreting coherency-driven modifications of solidification pathways in alloys.

## 2. Theoretical model

Our study considers binary alloy systems consisting of two elements  $A$  and  $B$ . These systems form solid phases at low temperatures:  $A$ -rich  $\alpha$  phase and  $B$ -rich  $\beta$  phase with limited solubility of the other element. The systems can form an invariant point in which both solid phases are in equilibrium with a liquid phase,  $L$ . Our goal is to construct a theoretical model that provides conditions for such three-phase equilibria in the presence of a coherency

stress between the solid phases. To facilitate an analytical solution, we use simplifying assumptions about the system similar to those used in the original Cahn–Larché model for two-phase systems [10]. Specifically, we consider an infinite volume occupied by three phases; the solid phases are isotropic and linearly elastic; both solid phases have the same elastic properties described by, e.g., Young’s modulus  $E$  and Poisson’s ratio  $\nu$ . We further assume that the solid–liquid interface is incoherent so that the liquid phase does not support coherency stress. These assumptions allow the coherency energy,  $g_e$ , to depend only on the molar fractions of the solid phases ( $z_\alpha$  and  $z_\beta$ ) and the elastic energy associated with the lattice misfit,  $\epsilon$ :

$$g_e = z_\alpha z_\beta \frac{VE\epsilon^2}{(1-\nu)} = z_\alpha z_\beta \mathcal{W}, \quad (1)$$

where we introduce the coherency energy parameter  $\mathcal{W} = VE\epsilon^2/(1-\nu)$ . The coherency energy contribution,  $g_e$  is additive to the chemical energies of the phases represented by molar Gibbs free energies,  $g_i$  (with  $i \in \{\alpha, \beta, L\}$ ), that constitute the total molar energy of the system,  $g$ :

$$g(z_\alpha, z_\beta, x_\alpha, x_\beta, x_L) = z_L g_L(x_L) + z_\alpha g_\alpha(x_\alpha) + z_\beta g_\beta(x_\beta) + z_\alpha z_\beta \mathcal{W}, \quad (2)$$

where  $x_i$  is the composition of the  $i$ th phase expressed as a concentration of element  $B$ :  $x_i = N_i^B / (N_i^A + N_i^B)$  with  $N_i^A$  and  $N_i^B$  representing the number of moles of  $A$  and  $B$  elements in the  $i$ th phase. For an alloy of the overall composition,  $X$ , the phase molar fractions and compositions must satisfy the mass balance and the ranges given their definitions:

$$X = (1 - z_\alpha - z_\beta)x_L + z_\alpha x_\alpha + z_\beta x_\beta, \quad (3a)$$

$$z_\alpha + z_\beta + z_L = 1, \quad (3b)$$

$$0 \leq z_\alpha, z_\beta, z_L, x_\alpha, x_\beta, x_L, X \leq 1. \quad (3c)$$

Here,  $X$  is also expressed as a total molar concentration of  $B$ :  $X = N^B / (N^A + N^B)$  with  $N^A$  and  $N^B$  denoting the total moles of  $A$  and  $B$  elements in the alloy.

Minimizing the total Gibbs free energy in Equation (2) subject to the constraints in Equation (3) leads to the conditions for equilibrium in terms of  $z_i$  and  $x_i$  values. The global minimum can be found using the method of Lagrange multipliers. To this end, we introduce a Lagrangian:

$$\mathcal{L} = z_L g_L(x_L) + z_\alpha g_\alpha(x_\alpha) + z_\beta g_\beta(x_\beta) + \mathcal{W} z_\alpha z_\beta - \lambda(z_L x_L + z_\alpha x_\alpha + z_\beta x_\beta - X), \quad (4)$$

where  $\lambda$  is a Lagrange multiplier and the molar fraction of liquid is not independent  $z_L = (1 - z_\alpha - z_\beta)$ . Requiring partial derivatives of the Lagrangian with respect to the six independent variables ( $z_\alpha$ ,  $z_\beta$ ,  $x_\alpha$ ,  $x_\beta$ ,  $x_L$ ,  $\lambda$ ) to be equal to zero allows us to find the sought minimum of Gibbs free energy. Rearranging these six equations that set the partials equal to zero provides the following equations:

$$\begin{aligned} \frac{dg_L}{dx_L} &= \frac{dg_\alpha}{dx_\alpha} = \frac{dg_\beta}{dx_\beta} = \\ &= \frac{g_\alpha(x_\alpha) - g_L(x_L) + \mathcal{W} z_\beta}{x_\alpha - x_L} = \\ &= \frac{g_\beta(x_\beta) - g_L(x_L) + \mathcal{W} z_\alpha}{x_\beta - x_L}. \end{aligned} \quad (5)$$

Solving these equations for a specific set of functions describing the Gibbs free energies of individual phases (e.g., from thermodynamic databases) provides conditions for the thermodynamic equilibrium of the three phases. Note that, setting the coherency term to zero,  $\mathcal{W} = 0$ , in Equation (5), we recover classical equations that graphically manifest in the well-known common-tangent construction. The classical common-tangent rules also follow from Equation (5) for two-phase equilibria between the liquid and either of the solid phases because the additional coherency terms diminish when  $z_\alpha = 0$  or  $z_\beta = 0$ . With the non-zero coherency stress,  $\mathcal{W} \neq 0$ , and in the presence of both solid phases, the common tangent construction does not hold. Instead, the equilibrium between two solid phases is graphically represented by concave curves whose curvature depends on the magnitude of the coherency stress (see Figures 1 and 3), consistent with the results of Cahn and Larché [10].

Solving the equations (Equation (5)) with  $\mathcal{W} \neq 0$  for a range of alloy compositions and temperatures,  $(X, T)$  allows us to obtain phase equilibria in maps reminiscent of phase diagrams. We refer to them as *phase equilibria maps* rather than phase diagrams because these maps display phases in equilibrium yet do not possess such features of classical phase diagrams as the lever rule. Section 3 presents implementation and results of this approach for specific eutectic- and peritectic-forming binary systems.

### 3. Results

#### 3.1. Specific binary systems and functional forms for Gibbs free energies

We present two case studies that use the general theoretical model presented in the previous section to elucidate the impact of coherency stress on invariant points. The two case studies consider (i) a eutectic-forming binary alloy system and (ii) a binary system with a peritectic. To focus on the fundamental and qualitative effects of the coherency stress, we consider simple quadratic functions to describe the molar Gibbs free energies of the solid phases ( $\alpha$  and  $\beta$ ) parametrized by unique sets of scalar parameters,  $x^0$ ,  $a$ ,  $b$ :

$$g_\alpha = a(x_\alpha - x_\alpha^0)^2 + b_\alpha \quad (6a)$$

$$g_\beta = a(x_\beta - x_\beta^0)^2 + b_\beta \quad (6b)$$

We use a similar functional form for the liquid phase,  $L$  with the addition of a linear dependence on temperature,  $T$ :

$$g_L = a(x_L - x_L^0)^2 + b_L - \phi T, \quad (7)$$

where the  $\phi$  coefficient controls the rate at which the liquid phase is stabilized with increasing temperature and thus implicitly encodes the entropy of melting. In both Equations (6) and (7), the  $b_i$  parameter sets the reference free energy of each phase at its equilibrium composition.

This parametrization of the Gibbs free energy functions allows us to investigate both eutectic and peritectic-forming binary systems by a suitable selection of the  $x^0$  parameters that control the position of the parabolic curves. A eutectic point can be introduced by setting  $x_\alpha^0 < x_L^0 < x_\beta^0$ , whereas  $x_L^0 < x_\alpha^0 < x_\beta^0$  represents a system with a peritectic point. Since the specific curvature of the Gibbs free energy curves does not affect the results sought in this study, the curvature parameter  $a$  is adopted identical for all three functions. Our parameter selection represents binary systems where the melting points of the solid phases are comparable and are both much higher than the invariant points.

Although simple, this parametrization allows us to elucidate fundamental effects of coherency stress on three-phase equilibria at invariant points. To this end, we substitute these Gibbs free energy functions (Equations (6) and (7)) into Equation (5) and solve the resulting system of equations for a given

combination of alloy composition,  $X$ , temperature,  $T$ , and coherency term,  $\mathcal{W}$ . Solving the equations provides us with molar fractions,  $z_i$  and concentrations  $x_i$  (e.g., of element  $B$ ) of the phases in equilibrium under given conditions. Obtaining phase molar fractions for systematically varied alloy compositions,  $X$ , and temperatures,  $T$ , allow us to construct phase equilibria maps to visualize the impact of coherency stress on eutectic and peritectic regions of binary phase diagrams.

#### 3.2. Computer implementation

To streamline the solution of the systems of equations for many combinations of  $(X, T)$  required for the construction of phase equilibria maps, we developed the following algorithm implemented in Python.

1. Solve equations for pairwise two-phase equilibria in solid phases and the liquid ( $\alpha-L$ ,  $\beta-L$ ).
2. Solve equations for two-phase equilibria including the two solid phases ( $\alpha-\beta$ ).
3. Solve equations for three-phase equilibria including all three phases ( $\alpha-\beta-L$ ).
4. Calculate the Gibbs free energies corresponding to seven potential cases of equilibrium: three single-phase, three two-phase, and one three-phase conditions.
5. For each overall alloy composition,  $X$ , and temperature,  $T$ , find the equilibrium that corresponds to the lowest Gibbs free energy and store the corresponding label that lists phases with non-zero molar fractions.
6. Visualize the results as fields of labels that list the phases in equilibrium.

Our implementation leverages the library `sympy` [34] for symbolic solution of systems of equations in Python. The next subsections demonstrate the application of this approach and its computer implementation to simple eutectic and peritectic systems. Table 1 lists the numerical parameters adopted for the two systems. Since  $b_\alpha = b_\beta \equiv b$  adopted for this study, we express the coherency energy parameter,  $\mathcal{W}$ , in units of  $b$  in all subsequent analysis to present a dimensionless measure of the elastic strain energy relative to the characteristic chemical free energy of the solid phases. The numerical value for the  $\phi$  coefficient for both case studies was adopted to obtain invariant points in a temperature range representative of real metallic systems (e.g., Cu–Ag, see Figure 5(a)).

Table 1: Parameters adopted for the Gibbs energy functions of the two systems.

| Parameter                | $x_\alpha^0$ | $x_\beta^0$ | $x_L^0$ | $a$ | $b_\alpha$ | $b_\beta$ | $b_L$ | $\phi$ |
|--------------------------|--------------|-------------|---------|-----|------------|-----------|-------|--------|
| <b>Eutectic system</b>   | 0.2          | 0.8         | 0.5     | 50  | 21         | 21        | 40    | 0.0167 |
| <b>Peritectic system</b> | 0.5          | 0.8         | 0.3     | 50  | 21         | 21        | 40    | 0.0167 |

### 3.3. Case study 1: Eutectic system

We first consider the application of our theoretical model (Section 2) for a binary system that includes a eutectic point in its conventional stress-free phase diagram. To ensure eutectic equilibrium, we set  $x_\alpha^0 < x_L^0 < x_\beta^0$  in our Gibbs free energy parametrization (Equations (6) and (7)). We then analyze the Gibbs free energy curves corresponding to different combinations of the phases (Figure 1) and phase equilibria maps for a full range of overall alloy compositions,  $X \in [0, 1]$ , and a temperature range, 850 K to 1350 K, which covers the conditions for three-phase eutectic equilibria in this system.

The Gibbs free energy curves clearly show the impact of coherency strain effects on the energetics of the system (Figure 1). We analyze the Gibbs free energy curves at three magnitudes of the  $\mathcal{W}$  parameter and at three temperatures: (i) below, (ii) equal to, and (iii) above the eutectic temperature,  $T_E$ , in the stress-free phase diagram. In the absence of the coherency stress ( $\mathcal{W} = 0$ , Figure 1a), our calculations reproduce the traditional common-tangent construction. The lowest energy configurations follow the standard sequence:  $\alpha$  and  $\beta$  at  $T = T_1 < T_E$ , three-phase equilibrium at  $T = T_2 = T_E$ , and pairwise liquid–solid equilibria at  $T = T_3 > T_E$ .

The addition of the coherency stress ( $\mathcal{W} > 0$ , Figure 1b,c) leads to distinct changes. First, the curve representing equilibrium between the solid phases arches upward instead of the classical linear common tangent. Consequently, the liquid phase becomes energetically favorable at temperatures where it would be unstable in a classical, coherency-free system. For example, the liquid curve lies below the coherent two-solid curve even at  $T \geq T_E$  (first two rows in Figure 1b,c). Three-phase equilibria are also observed as the lowest energy configuration at a temperature below  $T_E$  (see red segment in Figure 1b,c) and, even more interestingly, for a range of compositions. Finally, this compositional range of three-phase equilibria is narrower for a greater magnitude of the  $\mathcal{W}$  parameter: compare the red segments in Figure 1b vs. Figure 1c.

By systematically solving the equilibrium equations over the full range of temperatures and compositions, we translate the energetic shifts observed in the Figure 1 into the phase equilibria maps presented in Figure 2. These maps visualize the stability domains of the liquid ( $L$ ), solid ( $\alpha$ ,  $\beta$ ), and mixed-phase regions as a function of the coherency term,  $\mathcal{W}$ . In the stress-free limit ( $\mathcal{W} = 0$ , Figure 2(a)), our calculated map reproduces a classical binary eutectic phase diagram. The three phases ( $\alpha$ ,  $\beta$ , and  $L$ ) coexist only at a single eutectic temperature consistent with the classical Gibbs phase rule.

Introducing coherency stress fundamentally alters the topology of the phase equilibria maps. As  $\mathcal{W}$  increases, the eutectic equilibrium expands into a distinct three-phase field ( $\alpha+\beta+L$ ). This region of three-phase coexistence grows significantly in area and height with increasing coherency term. Its existence over a range of temperatures and compositions visually confirms the three-phase equilibrium in a range of compositions observed with the curves in Figure 1. The phase equilibria maps show that the narrowing of the three-phase equilibrium segment in composition is a consequence of the progressive depression of solidification temperatures with increasing  $\mathcal{W}$ . Indeed, as predicted by the Gibbs free energy curves, the liquidus lines (boundaries between  $L$  and two-solid regions) shift downward and the "eutectic" region moves to progressively lower temperatures as the coherency penalty increases.

### 3.4. Case study 2: Peritectic system

We next use our model and implementation for the binary system that includes a peritectic point in its conventional coherency-free phase diagram. To this end, we set  $x_L^0 < x_\alpha^0 < x_\beta^0$  in the functions describing the Gibbs free energies of the phases (Equations (6) and (7)). As for the eutectic case, Table 1 lists a specific set of values adopted for the parameters defining the  $g$  functions. This parametrization ensures a peritectic point within the considered temperature range (850 K to 1350 K).

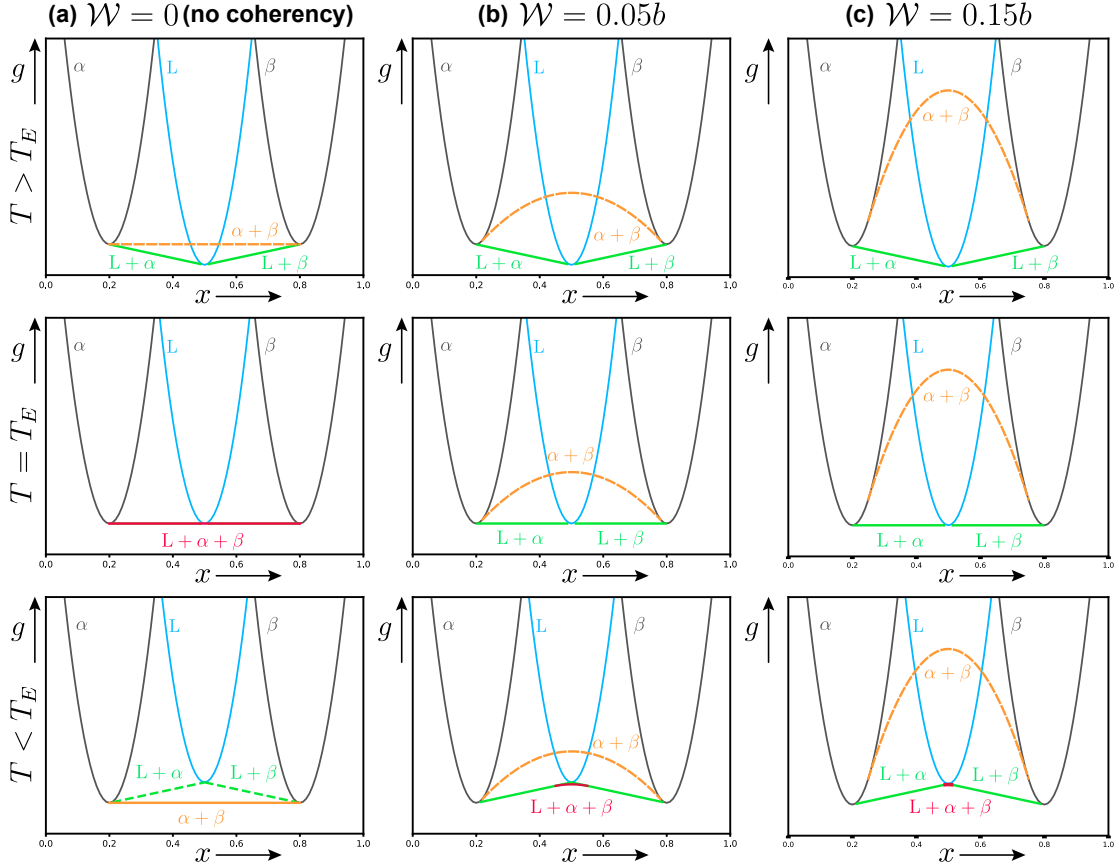


Figure 1: Gibbs free energy curves at three representative temperatures relative to the eutectic temperature in the stress-free system ( $T_E$ ) obtained with various coherency magnitudes,  $\mathcal{W}$ , expressed in terms of the reference free energy parameter of the solid phases ( $b = b_\alpha = b_\beta$ ).

Figure 3 illustrates the impact of coherency strain on the Gibbs free energy curves of the peritectic system. We track the evolution of the curves with coherency at three temperatures relative to the stress-free peritectic temperature,  $T_P$ . In the stress-free limit ( $\mathcal{W} = 0$ , left column), the system behaves classically. Unlike the eutectic case, where liquid–solid equilibria are both permissible (depending on the composition) at high temperatures, the peritectic system is defined by a competition between them. At temperatures below the peritectic point, the common tangent for  $\beta+L$  is above the  $\alpha+L$  and  $\alpha+\beta$  lines. Introducing coherency stress ( $\mathcal{W} > 0$ ) changes equilibria in a manner distinct from the eutectic case due to the underlying arrangement of the free energy curves. In the peritectic system, the liquid curve is positioned to the side of the solid curves rather than between them as in the eutectic system. Consequently, when the coherent solid

curve ( $\alpha + \beta$ ) arches upward due to the strain energy, it does not intersect the liquid curve to form a broad three-phase region. This asymmetry leads to conceptually distinct behavior in the peritectic system: the lack of stabilization of the three-phase configuration by coherency stress observed in the eutectic system.

Phase equilibria maps obtained for this peritectic system (Figure 4) confirms that no three-phase configuration represents the global energy minimum across the full range of temperatures and alloy compositions consistent with the analysis at three selected temperatures in Figure 3. While coherency stress changes topology of the phase equilibria regions, there is no longer field for three-phase equilibria found in the eutectic system. Indeed, the coherency stress penalizes the two-solid equilibrium, whose region shrinks as the coherency stress increases. The  $\alpha+\beta$  region is taken over by fields cor-

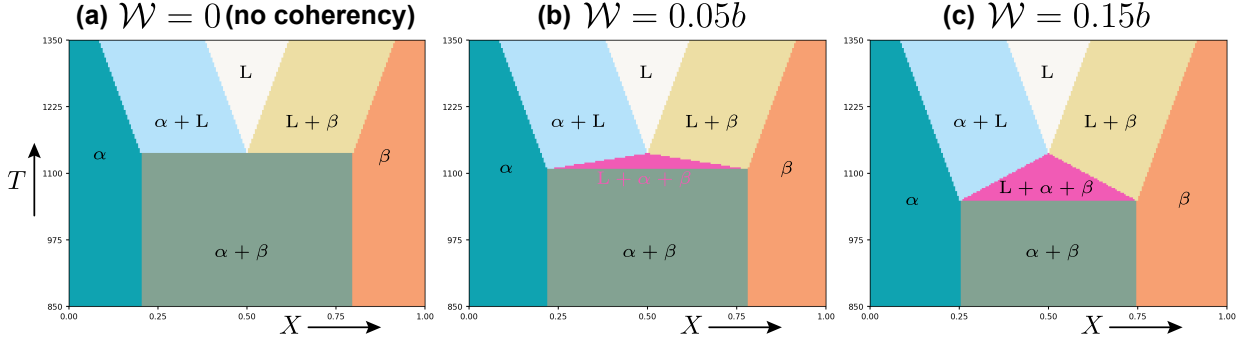


Figure 2: Phase equilibria maps for various coherency magnitudes,  $\mathcal{W}$ , expressed in terms of the reference free energy parameter of the solid phases ( $b = b_\alpha = b_\beta$ ).

responding to single  $\alpha$  and  $\beta + L$  equilibria, whose energetics are not affected by the presence of the coherency stress between the two solid phases.

## 4. Discussion

### 4.1. Asymmetry in coherency effects in eutectic and peritectic systems

The central result of this study is that coherency stress affects eutectic and peritectic invariant equilibria in conceptually different ways. In eutectic systems, the classical invariant point expands into a finite three-phase ( $\alpha + \beta + L$ ) equilibrium field. In peritectic systems, coherency stress progressively destabilizes the two-solid ( $\alpha + \beta$ ) equilibrium and can entirely suppress the peritectic equilibrium. This asymmetry has not been previously identified and is the main outcome of the present work extending the Cahn–Larché framework [10] to three-phase equilibria involving a liquid.

Violation of the Gibbs phase rule and breakdown of the common-tangent construction in the presence of coherency stress observed in this study is consistent with prior findings in solid-state systems [10, 11, 35]. The  $z_\alpha z_\beta \mathcal{W}$  term introduces explicit dependence of the system free energy on phase fractions, which is absent in classical thermodynamics, where free energy is a function of composition and temperature only. The present work shows that this mechanism operates in the same way when one of the coexisting phases is a liquid: the elastic energy penalizes the coherent solid–solid pair regardless of whether the third phase is solid or liquid, and this penalty is sufficient to expand a classical eutectic point into a three-phase field. This result is consistent with the findings of Roytburd and Sung

[26], whose model shares with the present work a dependence of the two-phase free energy on phase fractions through a fraction-dependent interaction term. However, in their treatment, elastic energy arises from direct and substrate-mediated epitaxial strain and can be either positive or negative, which determines the topological outcome. In the present work, the  $\mathcal{W}$  term originates from lattice misfit between bulk solid phases without any external constraint and is thus strictly non-negative. As a result, the topological outcome is controlled by the geometric relationship between the liquid and solid compositions, which in turn gives rise to the eutectic–peritectic asymmetry identified here.

The asymmetry originates from the geometric relationship between the compositions of the liquid and the two solids at the invariant condition. In a eutectic system, the liquid composition lies between those of the two solids ( $x_\alpha^0 < x_L^0 < x_\beta^0$ ). When coherency stress raises the free energy of the  $\alpha + \beta$  mixture, the system can lower its total energy by replacing some of the strained solid with stress-free liquid. Because  $x_L^0$  lies between  $x_\alpha^0$  and  $x_\beta^0$ , the liquid is compositionally positioned to substitute for either solid. This thermodynamic route stabilizes a three-phase field that extends to temperatures well below the stress-free eutectic point. In a peritectic system, the liquid composition lies outside the range spanned by the two solids ( $x_\alpha^0 < x_\beta^0 < x_L^0$  or  $x_L^0 < x_\alpha^0 < x_\beta^0$ ). The liquid cannot compositionally substitute for the solid–solid mixture as in the eutectic case. Instead, the coherency penalty on  $\alpha + \beta$  is relieved by expanding the single-phase and solid–liquid two-phase fields at the expense of the two-solid field. This behavior progressively eliminates the  $\alpha + \beta$  equilibrium instead of stabilizing a three-phase region.

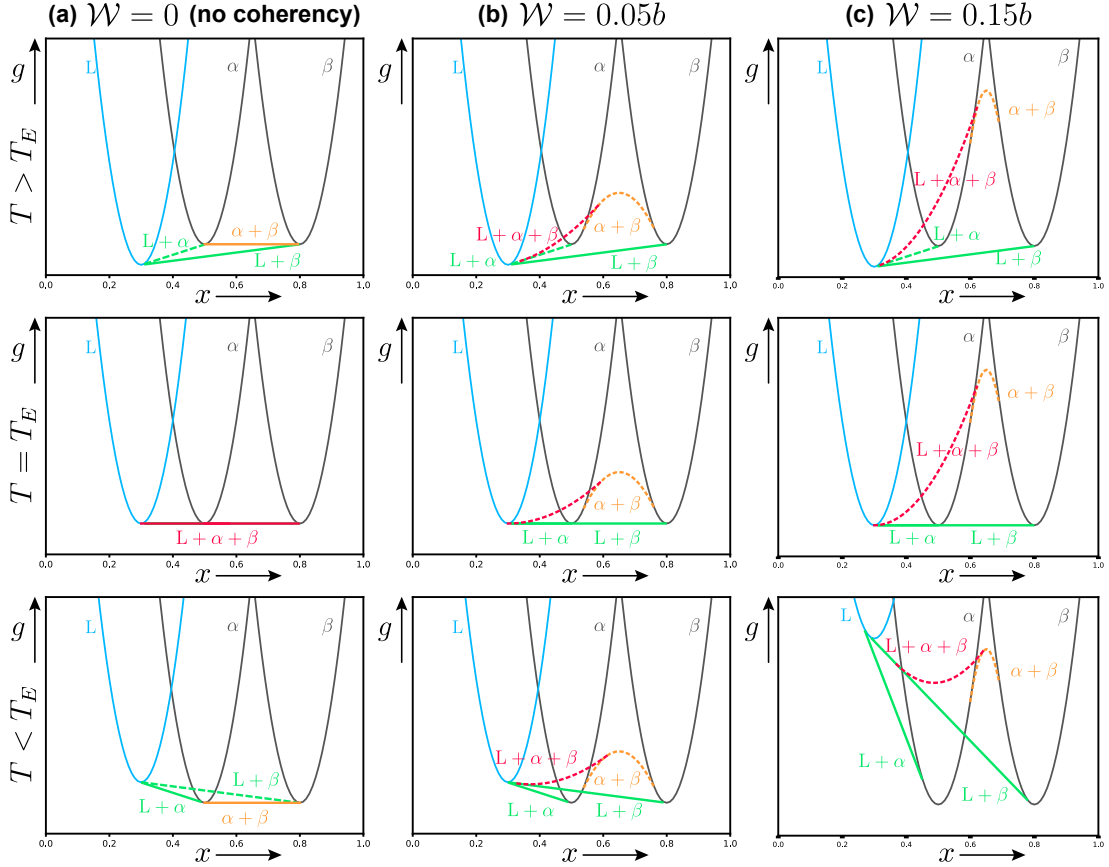


Figure 3: Gibbs free energy curves at three representative temperatures relative to the peritectic temperature in the stress-free system ( $T_P$ ) obtained with various coherency magnitudes,  $\mathcal{W}$ , expressed in terms of the reference free energy parameter of the solid phases ( $b = b_\alpha = b_\beta$ ).

#### 4.2. Limitations

The model employs simplifications whose consequences are discussed below.

First, the Gibbs free energy functions are represented as symmetric parabolas (Equations (6) and (7)) centered on the equilibrium composition of each phase. This approximation omits the configurational entropy of mixing,  $k_B T[x \ln x + (1 - x) \ln(1 - x)]$ , which introduces logarithmic singularities at  $x \rightarrow 0$  and  $x \rightarrow 1$ . In a realistic free energy function, these singularities steepen the free energy curves near the pure-component limits and affect the precise positions of phase boundaries at dilute compositions. However, the topological changes discussed in Section 4.1 are driven by the  $z_\alpha z_\beta \mathcal{W}$  term independent of the functional form of the chemical free energy. We expect the qualitative predictions to be robust to the choice of free energy parameterization, though quantitative phase

boundary positions will shift when realistic thermodynamic functions are used (e.g., from CALPHAD databases [36]).

Second, both solid phases are assumed to have identical, isotropic elastic constants. This assumption, inherited from the original Cahn–Larché model [10], simplifies the elastic energy to the Vegard-type expression used here (Equation (1)) but neglects elastic inhomogeneity between phases, which can introduce additional compositional and morphological dependencies [11, 37]. Relaxing this assumption (e.g., leveraging recent developments [14, 15, 16]) would modify the functional form of the elastic energy but would not eliminate the phase-fraction dependence that is responsible for the topological effects.

Third, the equilibrium maps presented here represent global free energy minima at each  $(X, T)$  point. Johnson and Voorhees [11, 12] showed that

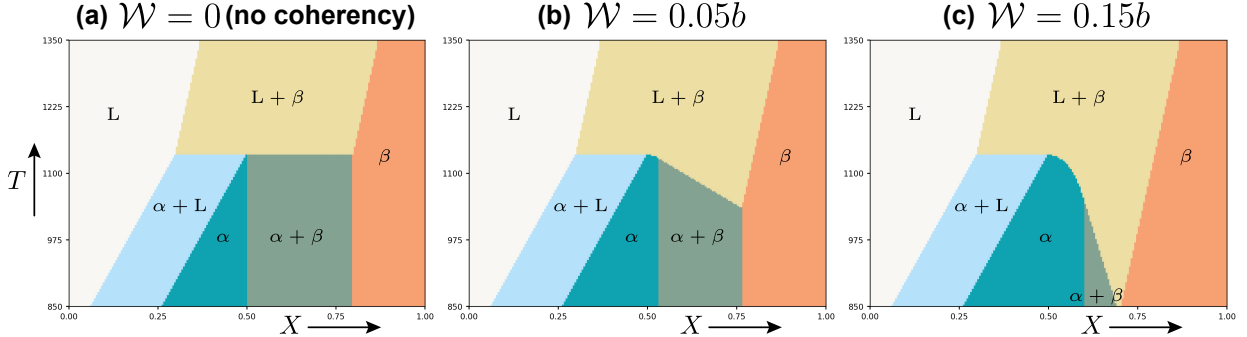


Figure 4: Phase equilibria maps for various coherency magnitudes,  $\mathcal{W}$ , expressed in terms of the reference free energy parameter of the solid phases ( $b = b_\alpha = b_\beta$ ).

coherent two-phase systems can admit multiple linearly stable equilibrium states under identical thermodynamic conditions, which is not observed in classical (incoherent) thermodynamics. The same multiplicity is expected in the three-phase case treated here. Experimentally, which equilibrium state is realized depends on the kinetic pathway: solidification rate, nucleation sequence, and thermal history – all influence whether the system reaches the global minimum or is trapped in a metastable configuration. The maps in Figures 2 and 4 should therefore be interpreted as thermodynamic bounds. The equilibrium states accessible during actual solidification may be a subset of those bounds.

#### 4.3. Relevance to real systems and outlook

To assess the practical magnitude of the predicted effects, we applied the model to the Cu–Ag eutectic system. We extracted the Gibbs free energy minima for the Cu-rich and Ag-rich solid solutions at 1000 K from Thermo-Calc and matched our parabolic free energy functions to these minima. The elastic strain energy was evaluated using the elastic properties of copper ( $E = 110$  GPa,  $\nu = 0.34$ ) and a variable lattice misfit between the equilibrium Cu-rich and Ag-rich phases (Figure 5). For a realistic coherent misfit of 1% representative of the strain ( $\epsilon \approx 0.01$ ) that can be sustained elastically without misfit dislocations in typical metallic systems, the resulting  $\mathcal{W}$  is small relative to the characteristic chemical free-energy differences (Figure 5(b)). Pushing the misfit even to the upper bound ( $\epsilon = 0.05$ ) of the small-strain assumptions underlying the Cahn–Larché formulation, the elastic contribution to the free energy remains modest compared to the chemical components, and the deviation of the coherent free energy from the classical

common tangent for the  $\alpha + \beta$  mixture is correspondingly small (Figure 5(c)). Consequently, the predicted broadening of the  $L + \alpha + \beta$  field and the depression of solidification temperatures are minor for this system.

The scaling  $\mathcal{W} \propto E\epsilon^2$  indicates that substantially larger effects are expected in systems combining high elastic stiffness with large sustainable coherent misfit. Candidate systems include refractory alloys based on Mo, W, or Nb (high  $E$ , moderate  $\epsilon$ ), ordered intermetallics with large lattice parameter differences between disordered and ordered phases, and strain-engineered semiconductor alloys such as Ge–Sn [5] where coherent epitaxy can be maintained over thicknesses sufficient for bulk-like thermodynamic behavior. In such systems, the predicted three-phase field broadening could be large enough to measurably alter solidification paths.

Direct experimental validation of the invariant-point-to-field transformation remains an open challenge, but indirect evidence from solid-state systems supports the underlying physics. Coherency-modified phase boundaries have been quantitatively documented in LiFePO<sub>4</sub> battery cathodes, where strain suppresses phase separation and produces upward-sloping voltage plateaus inconsistent with classical common-tangent predictions [38]. In thermoelectric PbTe–PbS alloys, coherency strain qualitatively alters the miscibility gap, stabilizing metastable solid solutions that decompose upon annealing into coherent nanoscale precipitates [39]. In Mg<sub>2</sub>Si–Mg<sub>2</sub>Sn, coherent strain energy has been shown to entirely suppress the chemical spinodal and phase decomposition [40]. These solid-state examples confirm that coherency stress can produce topological changes to phase diagrams in real materials. In the context of solidification, the  $L \rightarrow$

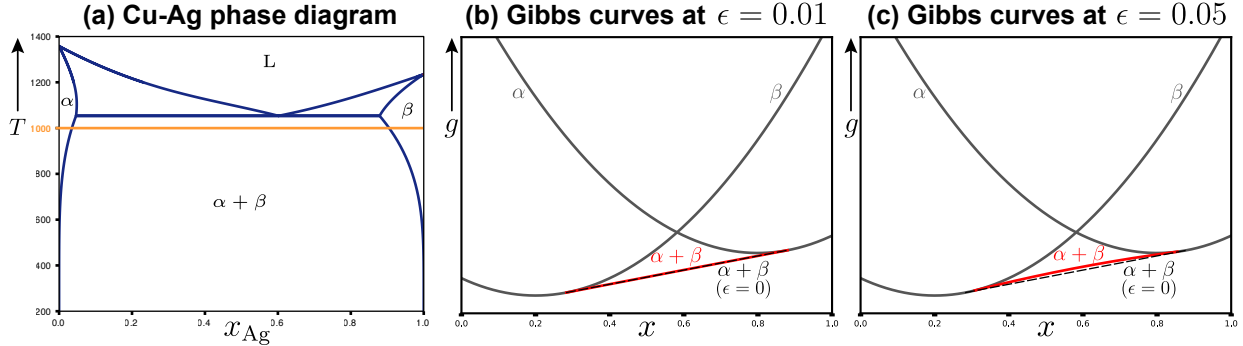


Figure 5: Assessment of predicted effects for a realistic eutectic system exemplified by Cu–Ag: (a) phase diagram and parabolic approximations of the Gibbs free energies with deviations from the common tangent corresponding to (b) realistic lattice misfit of 1 % and (c) its theoretical upper bound 5 %. The common tangent for  $\alpha + \beta$  is shown as a dashed line in (b,c).

$\gamma + \gamma'$  eutectic in Ni-base superalloys involves coherent solid phases with approx. 0.5 % lattice misfit, and microstructural observations indicate that this transformation occurs over a temperature range rather than at a single isotherm [41, 2]. This behavior is consistent with the invariant field predicted in this study, however, other factors (multicomponent thermodynamics, kinetics) may also play a role.

The present framework could benefit from extensions that would bring it closer to experimental relevance. Incorporating realistic free energy functions from CALPHAD databases [36] would enable quantitative predictions for specific alloy systems. Marschall et al. [42] have recently demonstrated such integration for solid-state coherent equilibria in multi-component alloys, which could serve as a viable pathway for extending the present framework to realistic systems. Allowing for partial coherency through a composition- or size-dependent loss-of-coherency criterion would bridge the gap between the fully coherent limit treated here and the incoherent limit assumed in conventional phase diagram calculations. Coupling the modified equilibrium conditions to a solidification model (e.g., Scheil-type calculation [1]) would predict how the altered equilibria affect freezing paths, microsegregation, and microstructural length scales in casting and additive manufacturing [6]. Finally, phase-field simulations that incorporate the  $z_\alpha z_\beta \mathcal{W}$  energy could capture morphological evolution during solidification through coherent three-phase regions, including the competition between equilibrium and metastable states discussed in Section 4.2.

## 5. Conclusions

We extended the Cahn–Larché thermodynamic framework to binary alloys in which two coherent solid phases coexist with an incoherent liquid and applied the model to eutectic- and peritectic-forming systems. The principal findings are as follows.

1. Coherency stress transforms the classical eutectic invariant point into a finite three-phase ( $L + \alpha + \beta$ ) equilibrium field spanning a continuous range of compositions and temperatures. This field expands with increasing coherency strain energy.
2. In peritectic systems, coherency stress does not stabilize a three-phase field. Instead, it progressively destabilizes the two-solid ( $\alpha + \beta$ ) equilibrium, which is consumed by single-phase and solid–liquid fields and can be suppressed entirely at sufficiently large strain energies.
3. This eutectic–peritectic asymmetry is governed by the geometric relationship between the stress-free compositions of the phases: when the liquid composition lies between those of the two solids (eutectic), the liquid can act as a thermodynamic buffer against the coherency penalty; when it lies outside (peritectic), it cannot.
4. Application to the Cu–Ag eutectic with realistic elastic properties shows that the topological transformation from invariant point to invariant field occurs even when the quantitative shifts in phase boundaries are small, confirming that the effect is qualitative in nature.

These results establish that coherency stress between solid phases can fundamentally alter three-phase equilibria involving a liquid in binary alloys and suggest that such effects may be significant in systems with large coherent misfits, such as refractory alloys, ordered intermetallics, and strain-engineered semiconductors.

## Acknowledgments

This material is based upon work supported by the National Science Foundation under Award No. 2441813.

## References

- [1] D. A. Porter, K. E. Easterling, Phase transformations in metals and alloys (revised reprint), CRC press, 2009.
- [2] T. M. Pollock, S. Tin, Nickel-based superalloys for advanced turbine engines: chemistry, microstructure and properties, *Journal of propulsion and power* 22 (2) (2006) 361–374.
- [3] A. Zunger, D. Wood, Structural phenomena in coherent epitaxial solids, *Journal of crystal growth* 98 (1-2) (1989) 1–17.
- [4] G. Stringfellow, Epitaxial growth of metastable semiconductor alloys, *Journal of Crystal Growth* 564 (2021) 126065.
- [5] D. Jung, S. S. Behara, A. Van der Ven, Phase stability and chemomechanics in the ge–sn alloy, *Acta Materialia* 299 (2025) 121369.
- [6] T. DebRoy, H. L. Wei, J. S. Zuback, T. Mukherjee, J. W. Elmer, J. O. Milewski, A. M. Beese, A. d. Wilson-Heid, A. De, W. Zhang, Additive manufacturing of metallic components—process, structure and properties, *Progress in materials science* 92 (2018) 112–224.
- [7] F. Larché, J. W. Cahn, A linear theory of thermochemical equilibrium of solids under stress, *Acta metallurgica* 21 (8) (1973) 1051–1063.
- [8] F. Larché, J. W. Cahn, A nonlinear theory of thermochemical equilibrium of solids under stress, *Acta Metallurgica* 26 (1) (1978) 53–60.
- [9] F. Larché, J. W. Cahn, Overview no. 41 the interactions of composition and stress in crystalline solids, *Acta metallurgica* 33 (3) (1985) 331–357.
- [10] J. Cahn, F. Larché, A simple model for coherent equilibrium, *Acta metallurgica* 32 (11) (1984) 1915–1923.
- [11] W. C. Johnson, P. Voorhees, Phase equilibrium in two-phase coherent solids, *Metallurgical Transactions A* 18 (1987) 1213–1228.
- [12] W. Johnson, P. Voorhees, Coherent phase diagrams, *Bulletin of Alloy Phase Diagrams* 9 (3) (1988) 208–215.
- [13] S. Shi, J. Markmann, J. Weissmüller, Verifying larché-cahn elasticity, a milestone of 20th-century thermodynamics, *Proceedings of the National Academy of Sciences* 115 (43) (2018) 10914–10919.
- [14] R. Spatschek, G. Gobbi, C. Hüter, A. Chakrabarty, U. Aydin, S. Brinckmann, J. Neugebauer, Scale bridging description of coherent phase equilibria in the presence of surfaces and interfaces, *Physical Review B* 94 (13) (2016) 134106.
- [15] A. T. Phan, A. E. Gheribi, P. Chartrand, Coherent phase equilibria of systems with large lattice mismatch, *Physical Chemistry Chemical Physics* 21 (20) (2019) 10808–10822.
- [16] A. T. Phan, A. E. Gheribi, P. Chartrand, Modeling of coherent phase transformation and particle size effect in lifepo<sub>4</sub> cathode material and application to the charging/discharging process, *Electrochimica Acta* 295 (2019) 632–644.
- [17] D. Wood, A. Zunger, Epitaxial effects on coherent phase diagrams of alloys, *Physical review letters* 61 (13) (1988) 1501.
- [18] D. M. Wood, A. Zunger, Coherent phase equilibria in strained binary alloys: Thermodynamic theory and first-principles calculation, *Physical Review B* 40 (6) (1989) 4062–4077.
- [19] S. S. Behara, J. C. Thomas, B. Puchala, A. Van der Ven, Chemomechanics in alloy phase stability, *Physical Review Materials* 8 (3) (2024) 033801.
- [20] B. Wang, L.-Q. Chen, Theory of strain phase equilibria and diagrams, *Acta Materialia* 274 (2024) 120025.
- [21] A. Khachaturyan, Theory of Structural Transformations in Solids, Dover Books on Engineering Series, Dover Publications, 2008.
- [22] Y. Wang, A. Khachaturyan, Microstructural evolution during the precipitation of ordered intermetallics in multiparticle coherent systems, *Philosophical Magazine A* 72 (5) (1995) 1161–1171.
- [23] Y. Wang, H.-Y. Wang, L.-Q. Chen, A. G. Khachaturyan, Microstructural development of coherent tetragonal precipitates in magnesium-partially-stabilized zirconia: A computer simulation, *Journal of the American Ceramic Society* 78 (3) (1995) 657–661.
- [24] C. Shen, Y. Wang, Phase-field microstructure modeling, in: Fundamentals of Modeling for Metals Processing, ASM International, 2009, pp. 297–311.
- [25] S. Rudraraju, A. Van der Ven, K. Garikipati, Mechanochemical spinodal decomposition: a phenomenological theory of phase transformations in multicomponent, crystalline solids, *npj Computational Materials* 2 (1) (2016) 1–9.
- [26] A. L. Roytburd, G. Sung, The formation of epitaxial eutectic modulated structures, *MRS Online Proceedings Library (OPL)* 311 (1993) 143.
- [27] A. Deymier, P. A. Deymier, K. Muralidharan, M. Latypov, Thermodynamics of the solid-liquid phase equilibrium of a binary system: Effect of a chemical reaction in the liquid and epitaxial strain in the solid, *Acta Materialia* 259 (2023) 119299.
- [28] A. C. Deymier, P. A. Deymier, M. Latypov, K. Muralidharan, Effect of stress on the dissolution/crystallization of apatite in aqueous solution: a thermochemical equilibrium study, *Philosophical Transactions of the Royal Society A* 381 (2250) (2023) 20220242.
- [29] J. A. Dantzig, M. Rappaz, Solidification, EPFL press, 2016.
- [30] M. C. Flemings, Solidification processing, *Metallurgical transactions* 5 (10) (1974) 2121–2134.
- [31] K. Jackson, J. Hunt, Lamellar and rod eutectic growth, in: Dynamics of curved fronts, Elsevier, 1988, pp. 363–376.
- [32] W. J. Boettinger, S. R. Coriell, A. Greer, A. Karma, W. Kurz, M. Rappaz, R. Trivedi, Solidification microstructures: recent developments, future directions, *Acta materialia* 48 (1) (2000) 43–70.

- [33] M. G. Worster, Convection in mushy layers, *Annual Review of Fluid Mechanics* 29 (1) (1997) 91–122.
- [34] A. Meurer, C. P. Smith, M. Paprocki, O. Čertík, S. B. Kirpichev, M. Rocklin, A. Kumar, S. Ivanov, J. K. Moore, S. Singh, et al., Sympy: symbolic computing in python, *PeerJ Computer Science* 3 (2017) e103.
- [35] C. Chiang, W. C. Johnson, Coherent phase equilibria in systems possessing a consolute critical point, *Journal of Materials Research* 4 (3) (1989) 678–687.
- [36] H. Lukas, S. G. Fries, B. Sundman, Computational thermodynamics: the Calphad method, Cambridge university press, 2007.
- [37] P. W. Voorhees, W. C. Johnson, The thermodynamics of elastically stressed crystals, in: *Solid state physics*, Vol. 59, Elsevier, 2004, pp. 1–201.
- [38] D. A. Cogswell, M. Z. Bazant, Coherency strain and the kinetics of phase separation in lifepo<sub>4</sub> nanoparticles, *ACS nano* 6 (3) (2012) 2215–2225.
- [39] S. N. Girard, K. Schmidt-Rohr, T. C. Chasapis, E. Hatzikraniotis, B. Njegic, E. Levin, A. Rawal, K. M. Paraskevopoulos, M. G. Kanatzidis, Analysis of phase separation in high performance pbte–pbs thermoelectric materials, *Advanced Functional Materials* 23 (6) (2013) 747–757.
- [40] S.-i. Yi, V. Attari, M. Jeong, J. Jian, S. Xue, H. Wang, R. Arroyave, C. Yu, Strain-induced suppression of the miscibility gap in nanostructured mg<sub>2</sub>si–mg<sub>2</sub>sn solid solutions, *Journal of Materials Chemistry A* 6 (36) (2018) 17559–17570.
- [41] N. D’Souza, J. Kelleher, C. Qiu, S.-Y. Zhang, S. Gardner, R. E. Jones, D. Putman, C. Panwisawas, The role of stress relaxation and creep during high temperature deformation in ni-base single crystal superalloys–implications to strain build-up during directional solidification, *Acta Materialia* 106 (2016) 322–332.
- [42] N. Marschall, J. Murugan, R. D. Kamachali, Incorporating elasticity into the thermodynamics and phase diagrams of multi-component systems, *Materialia* (2025) 102546.